Rapid Communications

Spin inertia of resident and photoexcited carriers in singly charged quantum dots

E. A. Zhukov,[1] E. Kirstein,[1] D. S. Smirnov,[2] D. R. Yakovlev,[1,2] M. M. Glazov,[2] D. Reuter,[3] A. D. Wieck,[4] M. Bayer,[1,2] and A. Greilich[1]

[1]*Experimentelle Physik 2, Technische Universität Dortmund, 44221 Dortmund, Germany*
[2]*Ioffe Institute, Russian Academy of Sciences, 194021 St. Petersburg, Russia*
[3]*Department Physik, Universität Paderborn, 33098 Paderborn, Germany*
[4]*Angewandte Festkörperphysik, Ruhr-Universität Bochum, 44780 Bochum, Germany*

(Received 2 July 2018; published 14 September 2018)

The spin dynamics in a broad range of systems can be studied using circularly polarized optical excitation with alternating helicity. The dependence of spin polarization on the frequency of helicity alternation, known as the spin inertia effect, is used here to study the spin dynamics in singly charged (In,Ga)As/GaAs quantum dots (QDs), providing insight into spin generation and accumulation processes. We demonstrate that the dependence of spin polarization in n- and p-type QDs on the external magnetic field has a characteristic V- and M-like shape, respectively. This difference is related to different microscopic mechanisms of the resident carriers' spin orientation. It allows us to determine the parameters of the spin dynamics both for the ground and excited states of singly charged QDs.

DOI: 10.1103/PhysRevB.98.121304

Long carrier spin coherence and spin relaxation times are the main prerequisites for a system to be suited for quantum information technologies [1,2]. The main route to extend these times is to isolate the studied system from its environment. At the same time, such isolation reduces the possibility for a fast state readout and manipulation. Carrier spins confined in low-dimensional semiconductor structures, in particular, singly charged (In,Ga)As quantum dots (QDs), offer a unique balance of accessibility and robustness [3]. The direct optical band gap with a giant optical dipole moment of a semiconductor QD [4] allows for exploiting the optical excitation, the exciton, as an auxiliary state for ultrafast conversion between the optical coherence of a laser pulse (picosecond duration) and the long-living spin coherence of an isolated resident carrier (microsecond coherence). This opportunity has triggered considerable activity in optical operations with QDs, including spin initialization [5], nondestructive readout [6], and spin manipulation [7].

The way the optical coherence is transferred to the spin coherence in a QD involves the process of optical orientation and excitation of a trion, the exciton which is bound to the resident carrier. After excitation, the trion recombines stochastically and leaves behind a polarized single carrier spin in the ground state, which is measured. Generally, the spin relaxation dynamics within a trion determines the final spin polarization. The standard optical methods to access the relaxation dynamics of resident spins are the Hanle effect [8] and time-resolved pump-probe techniques [9]. However, these techniques provide limited access to the spin generation process and dynamics of the photoexcited states [4].

In this Rapid Communication, we access the parameters of the spin dynamics in the trion by employing the recently developed *spin inertia* (SI) technique [10]. In SI, the spin dynamics in the system is related to the helicity modulation of the excitation polarization [11–13]. The maximal value of the spin polarization, created by the circularly polarized pump pulses, is then traced as a function of the helicity modulation frequency f_m. The spin polarization stays constant for $f_m \lesssim T_s^{-1}$, where T_s is the spin relaxation time of a carrier, and becomes reduced if the modulation frequency is larger than T_s^{-1}. The cutoff frequency defines the spin relaxation time [10,14].

In the presented experiment we study the spin relaxation in a model system, namely, an ensemble of singly charged (In,Ga)As/GaAs QDs, doped either with resident electrons or holes. The maximal spin polarization is determined by the interplay of the carrier spin generation and relaxation dynamics. Importantly, applying a longitudinal magnetic field, a substantial difference in the magnetic field behavior is observed for resident electron and hole spins. The origin of the observed difference and its relation to the SI represent the main topic of this Rapid Communication. Using the developed theory, we are able to exploit the full potential of the experiment. We describe the shape of the magnetic-field-dependent traces and extract information on the photoexcited carrier spin dynamics, which can be accessed from the signal accumulated long after the radiative trion decay. Furthermore, we determine spin relaxation times, longitudinal g-factor values, and hyperfine interaction strengths in the ground and excited states of the system.

We study n- and p-doped ensembles of singly charged self-assembled QDs. Both samples contain 20 layers of molecular beam epitaxy grown (In,Ga)As QDs separated by 60-nm GaAs barriers. The average QD density is about 10^{10} cm^{-2} per layer. The p-doped sample has a background level of p-type doping due to residual carbon impurities. The n-doped sample was obtained by incorporating δ sheets of Si 20 nm below each QD layer. The samples are mounted in the variable temperature insert of a magneto-optical bath cryostat ($T = 1.5$–300 K), and are excited by the laser close to the

maximum of the photoluminescence at 1.412 eV (878 nm) for the n-type QDs, and at 1.392 eV (891 nm) for the p-type QDs [15]. The laser spot diameters on the sample are 300 μm. As the samples are different in their doping types and concentrations, different excitation conditions are required for the strongest signal level. The magnetic field **B** is applied in Faraday geometry, along the optical z axis. Details on the sample characterization are given in Refs. [16,17].

The spin polarization is created by circularly polarized pump pulses of 1.5-ps duration emitted by a mode-locked Ti:sapphire laser operating at a repetition period $T_R = 13.2$ ns. The pump helicity is modulated at frequency f_m between σ^+ and σ^- polarization by an electro-optical modulator (EOM). Linearly polarized probe pulses measure the induced spin polarization along the optical axis via the ellipticity signal in transmission geometry analyzed by a quarter-wave plate and a Wollaston prism, using a balanced diode bridge [10]. This signal is called Faraday ellipticity (FE).

In the presented experiments, we fix the pump-probe delay at a negative value (−50 ps) and measure the FE dependence on the longitudinal magnetic field, applied along the excitation direction and orthogonal to the sample surface. Using the signal at negative time delay greatly simplifies the interpretation of the results, as it can only arise from the spin polarization of the resident long-living carriers. In the studied QDs the trion recombination time of 400 ps is much shorter than T_R [18].

Figures 1(a) and 1(b) demonstrate the measured FE as a function of magnetic field for different modulation frequencies for the n- and p-doped samples. We call this dependence a polarization recovery curve (PRC). For both samples the FE increases with an increase of magnetic field around $B = 0$. In the case of strong carrier localization, the dominant spin relaxation mechanism is the hyperfine interaction with host lattice nuclear spins. Application of the external magnetic field leads to an effective decoupling of the resident carrier spins from the nuclear spin bath and stabilizes the optically oriented spins along the z axis [10,20], so that the FE increases. At higher magnetic fields the behavior is different: The electron spin polarization saturates (in the range around 300 mT), while the hole spin polarization decreases after the initial increase and then saturates within a similar range of fields. The observed difference in the field dependencies of PRC is related to the type of carriers (electrons versus holes) and the spin relaxation dynamics in the trion states, which are schematically shown in the insets in Figs. 1(a) and 1(b).

The SI method gives access to the relaxation dynamics of the resident carriers, as shown by the exemplary data sets in Figs. 1(c) and 1(d). Figure 1(c) shows the f_m dependence of the FE at fixed magnetic field ($B = 300$ mT), extracted from the data shown in Fig. 1(a). Using the fit with the form [10]

$$\frac{\mathrm{FE}(f_m)}{\mathrm{FE}(0)} = \frac{1}{\sqrt{1+(2\pi f_m T_s)^2}}, \tag{1}$$

we determine the characteristic spin lifetime $T_s = 0.7$ μs of the resident electrons at a pump power of 4 mW [10]. In this case the spin polarization is far below the saturation level. The case of strong pumping is discussed in Ref. [14]. The value of T_s depends on the pump power due to the influence of the photoexcitation [10,21], hence, to determine

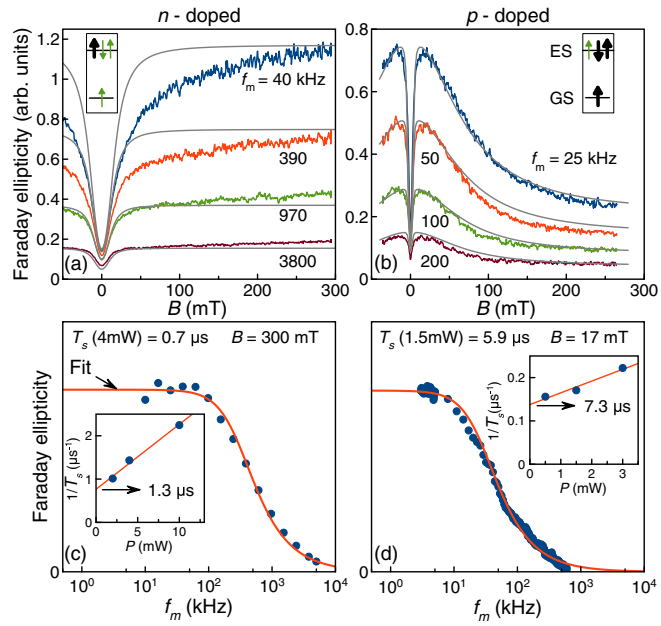

FIG. 1. Spin polarization of carriers as a function of magnetic field at different modulation frequencies of pump helicity: (a) n-doped sample, laser pump/probe power is 4/0.8 mW, $T = 6$ K; (b) p-doped sample, pump/probe power is 1.5/0.5 mW, $T = 1.7$ K. Gray curves are calculations after Eq. (2) with parameters given in Table I [19]. Insets show examples of possible ground (GS) and excited state (ES) spin configurations: Thin green and thick black arrows represent the electron and hole spins, respectively. (c) and (d) show the frequency dependencies of carrier spin polarizations at fixed magnetic field for the n- and p-doped samples, respectively. The red line is a fit by Eq. (1). Insets are linear extrapolations of the power-dependent spin lifetime T_s down to zero pump power giving the spin relaxation times in equilibrium $T_s^{(0)}$.

the longitudinal spin relaxation time in equilibrium $T_s^{(0)}$ we apply different pump powers P and extrapolate T_s down to zero power using a linear fit to the inverse of the data [see the inset in Fig. 1(c)]. It gives $T_s^{(0)} = 1.3$ μs for $B = 300$ mT in n-doped QDs. Figure 1(d) shows the corresponding frequency dependence for the p-doped sample around the maximum of the FE signal (at $B = 17$ mT) and $P = 1.5$ mW. The procedure described above yields $T_s = 5.9$ μs and $T_s^{(0)} = 7.3$ μs. This demonstrates the ability of SI to access very long spin relaxation times, exceeding T_R by almost three orders of magnitude. Spin relaxation times in the microsecond range are in good agreement with other measurements [13,15,21], while the difference from the results of Ref. [22] can be explained by the difference in the experimental protocol [23].

Importantly, the PRCs have different shapes for n- and p-doped samples. This situation changes with increasing temperature. Figure 2 demonstrates the evolution of the PRC for the p-doped sample at low modulation frequency $f_m = 2$ kHz, in the temperature range $T = 13$–20 K, where it is changing from an M to a V shape. In comparison, the temperature dependence of the V-type PRC for the n-type sample does not show a shape change (not shown here).

The full theory of SI is developed in the accompanying theoretical paper [14]. Here, we briefly summarize the main results and apply the developed theory to the description of

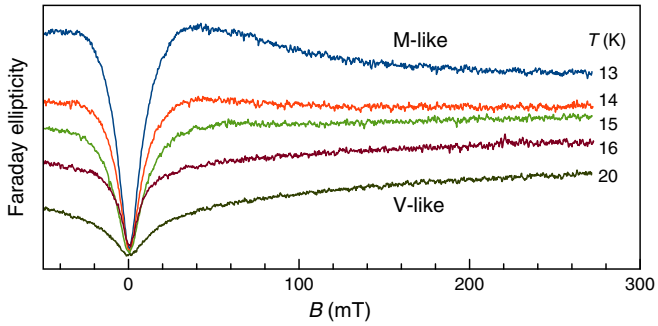

FIG. 2. Temperature dependence of PRC for the p-doped sample. Laser pump/probe power is 2/0.5 mW, $f_m = 2$ kHz.

the experimental results. The FE signal FE(f_m) is determined by the absolute value of the spin polarization at modulation frequency f_m. The spin dynamics for both types of carriers at small magnetic fields (<1 T) is dominated by the hyperfine interaction with the host lattice nuclei. The resident carrier spin in each QD precesses in the random Overhauser field, while the nuclear spins are subject to the Knight field created by the carrier and experience the quadrupolar interaction induced by the strain in QDs [24]. As a result, the spin polarization of an ensemble obeys a linear, but non-Markovian, equation of motion. In the model of Merkulov, Efros, and Rosen [25], two-thirds of the electron spin polarization is lost during the timescale of spin precession in the random Overhauser field ω_N^{-1}. The rest of the spin polarization is destroyed at longer times, such as the nuclear spin correlation time τ_c related, e.g., to the nuclear quadrupole interaction, or the spin relaxation time τ_s unrelated to the hyperfine interaction.

The spin dynamics can be described by the Green's function $G(f_m)$ in the frequency domain. A theoretical analysis of the SI measurement protocol [14] shows that the SI signal is proportional to

$$\mathrm{FE}(f_m) \propto QG(f_m). \tag{2}$$

Here, the factor Q is the probability of trion spin flip during its lifetime. According to the optical selection rules, trion excitation and recombination preserve the total spin along the excitation axis z. Therefore Q determines the efficiency of spin polarization in QDs [26]. Importantly, it is sensitive to the external magnetic field [27], which ultimately gives rise to the different shapes of PRC for different carriers. One can show that [14]

$$Q = \frac{\left(\omega_N^{\mathrm{T}}\tau_0/\lambda^{\mathrm{T}}\right)^2}{1+\left(\Omega_L^{\mathrm{T}}\tau_0\right)^2} + \frac{\tau_0}{\tau_s^{\mathrm{T}}}, \tag{3}$$

where ω_N^{T} is the characteristic trion spin precession frequency in the fluctuations of the Overhauser field along the z direction, λ^{T} is the parameter of the hyperfine interaction anisotropy of the trion, $\Omega_L^{\mathrm{T}} = g_{zz}^{\mathrm{T}}\mu_B B/\hbar$ is the trion spin precession frequency in the longitudinal external magnetic field with g_{zz}^{T} being the longitudinal g factor and μ_B being the Bohr magneton, and τ_s^{T} is the trion spin relaxation time unrelated to the hyperfine interaction. The laser repetition period T_R is assumed to be much longer than the trion lifetime τ_0.

TABLE I. Parameters of the resident and photoexcited carriers' spin dynamics, extracted from the fits in Fig. 1.

	g_{zz}	ω_N (MHz)	λ	τ_c (μs)	τ_s (μs)	τ_s^{T} (μs)
Electron	−0.61	70	1	0.2	0.5	< 1
Hole	−0.45	16	5	0.26	5.2	0.035

The Green's function of the spin dynamics accounting for the finite nuclear spin correlation time is [28]

$$G(f_m) = \frac{\tau_f \mathcal{A}}{1 - \mathcal{A}\tau_f/\tau_c}, \tag{4}$$

where $1/\tau_f = 1/\tau_s + 1/\tau_c - 2\pi i f_m$ and

$$\mathcal{A} = \int d\mathbf{\Omega}_N \mathcal{F}(\mathbf{\Omega}_N) \frac{1+\Omega_z^2\tau_f^2}{1+\Omega^2\tau_f^2}, \tag{5}$$

with $\mathbf{\Omega}_N$ being the frequency of spin precession in the random Overhauser field in a single QD and $\mathbf{\Omega} = \mathbf{\Omega}_N + \mathbf{\Omega}_L$ being the total spin precession frequency in a single QD. The distribution of the Overhauser field is Gaussian:

$$\mathcal{F}(\mathbf{\Omega}_N) = \frac{\lambda^2}{(\sqrt{\pi}\omega_N)^3} \exp\left(-\frac{\Omega_{N,x}^2 + \Omega_{N,y}^2}{\omega_N^2/\lambda^2} - \frac{\Omega_{N,z}^2}{\omega_N^2}\right), \tag{6}$$

where ω_N is the typical spin precession frequency in the QD ground state and λ describes the anisotropy of the hyperfine interaction. The latter is relevant ($\lambda > 1$) [29] for resident holes and for negatively charged trions, where the hole spin is unpaired, while the electrons form a singlet state with total spin zero [see the inset in Fig. 1(a)]. We stress that the parameters of the spin dynamics are different in the ground and excited states, so we used the superscript "T" in Eq. (3) for the parameters of the trion spin dynamics.

Equations (2)–(5) allow us to describe the experimental data shown in Fig. 1 and to determine the parameters of spin dynamics, which are summarized in Table I [19]. Below, we describe qualitatively how these parameters determine the PRC shape. As one can see from Eq. (2), the frequency dependence of the FE is described by the Green's function $G(f_m)$. In general, this dependence is governed by the coupled spin dynamics of carriers and nuclei and differs from Eq. (1). However, in sufficiently strong magnetic fields, where $\Omega_L > \omega_N$, Eq. (1) is valid, provided $T_s = \tau_s$. In this case, the cutoff in the frequency dependence of the FE signal yields the spin relaxation time in the ground state τ_s. All other parameters of the spin dynamics can be extracted from the PRC at small frequency.

At the smallest modulation frequencies $f_m \ll \tau_s^{-1}$, the FE signal does not depend on f_m and the Green's function at zero modulation frequency determines the average spin relaxation time $T_1 \equiv G(0)$. Therefore one simply has $\mathrm{FE}(f_m = 0) \propto Q(B)T_1(B)$, where both factors depend on magnetic field. The decomposition of FE into these two contributions is shown in Fig. 3. Here, the PRC curves calculated numerically (blue dashed curves with gray filling) are shown together with the dependencies $T_1(B)$ (black lines) and $Q(B)$ (red lines) calculated for the same parameters as in Table I.

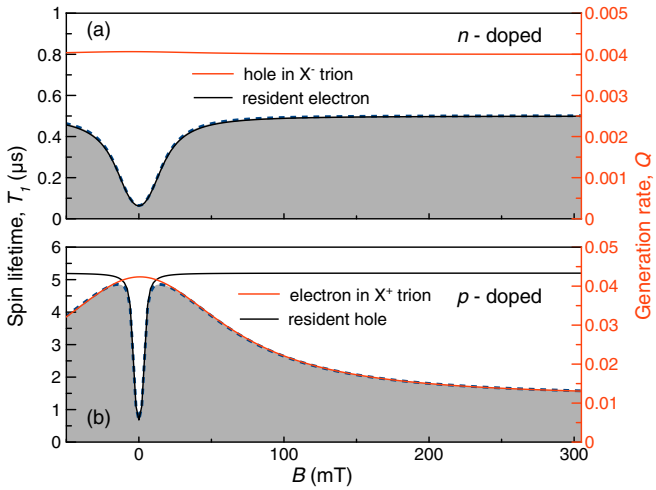

FIG. 3. Decomposition of the PRC (dashed blue lines, shaded for better visibility, arb. units) into magnetic field dependence of spin polarization of resident and photoexcited carriers: (a) n-doped, (b) p-doped samples. Black curves give the spin lifetime of resident carriers and red curves the generation rate Q determined by spin relaxation of the photoexcited carriers. The parameters of the calculation are the same as in Fig. 1.

The dip in the FE signals around zero magnetic field is determined by the dependence of T_1 on magnetic field. It is similar for both samples, as one can see in Fig. 3: The spin relaxation time increases with an increase of the longitudinal magnetic field, and then saturates. Its full width at half maximum is related to the longitudinal g-factor of the carrier and the characteristic nuclear field fluctuation ω_N as $\sim\hbar\omega_N/(g_{zz}\mu_B)$ [14]. Since the hyperfine interaction for electrons is stronger [30], the width of the T_1 curve is larger for the n-type sample than for the p-type one. We note that the saturation of the longitudinal spin relaxation time at large magnetic fields evidences the presence of a spin relaxation mechanism unrelated to the hyperfine interaction, which is described by the phenomenological time τ_s. The deviations of the modeled behavior from the experimental one for the n-type sample in the intermediate field range may be caused by specific correlations in the nuclear dynamics, such as quadrupole-induced spin relaxations, which are not included at this stage.

The ratio of the average spin relaxation time at large and zero magnetic fields is determined by the nuclear spin correlation time τ_c [14], thus, for resident electrons

$$\frac{T_1(B=\infty)}{T_1(B=0)} = 3 + 2\frac{\tau_s}{\tau_c}. \tag{7}$$

Therefore the increase of T_1 in both samples by more than three times indirectly evidences the finite hyperfine field correlation time. We note that the τ_c obtained from the fit is similar for both samples. This indicates that the nuclear spin dynamics is related to the quadrupole interaction, which is similar for both samples [31].

Figure 3 shows that the main difference between the FE dependence on B for the two samples is the spin generation rate, or the trion spin-flip probability $Q(B)$. In positively charged QDs the trion consists of two heavy holes in the singlet state and an electron [see the inset in Fig. 1(b)]. In this case, the trion spin relaxation at zero magnetic field is related to the hyperfine interaction of an unpaired electron spin with the host lattice nuclei in the QD. This is described by the first term in Eq. (3). With the increase of magnetic field, the electron spin gets effectively decoupled from the nuclear spin bath, and the trion spin-flip probability Q decreases, as shown in Fig. 3(b). The width of the dependence $Q(B)$ is given by $2\hbar/(g^{\mathrm{T}}_{zz}\mu_B\tau_0)$. Using $\tau_0 = 400$ ps [18], we find the trion g-factor $g^{\mathrm{T}}_{zz} = -0.4$, which is close to the bare electron g-factor. Moreover, assuming that the characteristic nuclear field is the same as for n-type QDs, $\omega^{\mathrm{T}}_N = 70$ MHz, we find the trion spin relaxation time unrelated to the hyperfine interaction, $\tau^{\mathrm{T}}_s = 35$ ns.

For negatively charged QDs the trion consists of two electrons in the singlet state and a hole with an unpaired spin, as shown in the inset in Fig. 1(a). In this case, the spin dynamics of the trion is determined by hole spin relaxation. The hyperfine interaction of a negatively charged trion is weaker than that of a positively charged trion. As a result, the trion spin relaxation in n-type QDs is unrelated to the hyperfine interaction and Q does not depend on B [see the red curve in Fig. 3(a)]. Mathematically, the second term in Eq. (3) dominates in this case, which allows us to estimate $\tau^{\mathrm{T}}_s < 1$ μs in the n-type sample.

Interestingly, the dependence $Q(B)$ can change with a temperature increase, provided τ^{T}_s depends on T. This takes place, for example, for the phonon-assisted spin relaxation mechanism, although the precise origin of τ^{T}_s for both types of quantum dots is not fully clear so far. The spin relaxation speeds up with an increase of temperature, so the dependence $Q(B)$ can become flat even for p-type QDs. This explains the change of the shape of the FE signal from M-like to V-like, shown in Fig. 2.

It is instructive to compare the SI technique with the spin noise technique [32,33]. Indeed, both give access to the Fourier transform of the spin dynamics Green's function, which can be measured for different magnetic fields. In fact, one can show that the spin noise spectrum is proportional to $\mathrm{Re}\, G_{zz}(f_m)$ [14]. Thus, it is characterized by the same parameters as given in Table I, but in a different way, which makes these two approaches complementary.

To conclude, we show that the SI measurement gives access to various parameters of the spin dynamics not only of the resident charge carriers but also of the photoexcited electron-hole complexes.

We acknowledge the financial support by the Deutsche Forschungsgemeinschaft in the frame of the International Collaborative Research Center TRR 160 (Projects A1 and A5), partial support by the Russian Foundation for Basic Research (Grant No. 15-52-12012), and Basis Foundation.

[1] D. Loss and D. P. DiVincenzo, Phys. Rev. A **57**, 120 (1998).

[2] T. D. Ladd, F. Jelezko, R. Laflamme, Y. Nakamura, C. Monroe, and J. L. O'Brien, Nature (London) **464**, 45 (2010).

[3] F. Henneberger and O. Benson, *Semiconductor Quantum Bits* (CRC Press, Boca Raton, FL, 2016).

[4] *Spin Physics in Semiconductors*, edited by M. I. Dyakonov (Springer, Berlin, 2017).

[5] M. Atatüre, J. Dreiser, A. Badolato, A. Högele, K. Karrai, and A. Imamoglu, Science **312**, 551 (2006).

[6] D. Kim, S. E. Economou, S. C. Bădescu, M. Scheibner, A. S. Bracker, M. Bashkansky, T. L. Reinecke, and D. Gammon, Phys. Rev. Lett. **101**, 236804 (2008).

[7] A. J. Ramsay, Semicond. Sci. Technol. **25**, 103001 (2010).

[8] W. Hanle, Z. Phys. **30**, 93 (1924).

[9] *Semiconductor Spintronics and Quantum Computation*, edited by D. D. Awschalom, D. Loss, and N. Samarth (Springer, Berlin, 2002).

[10] F. Heisterkamp, E. A. Zhukov, A. Greilich, D. R. Yakovlev, V. L. Korenev, A. Pawlis, and M. Bayer, Phys. Rev. B **91**, 235432 (2015).

[11] M. Ikezawa, B. Pal, Y. Masumoto, I. V. Ignatiev, S. Y. Verbin, and I. Y. Gerlovin, Phys. Rev. B **72**, 153302 (2005).

[12] I. A. Akimov, D. H. Feng, and F. Henneberger, Phys. Rev. Lett. **97**, 056602 (2006).

[13] F. Fras, B. Eble, P. Desfonds, F. Bernardot, C. Testelin, M. Chamarro, A. Miard, and A. Lemaître, Phys. Rev. B **84**, 125431 (2011).

[14] D. S. Smirnov, E. A. Zhukov, E. Kirstein, D. R. Yakovlev, D. Reuter, A. D. Wieck, M. Bayer, A. Greilich, and M. M. Glazov, Phys. Rev. B **98**, 125306 (2018).

[15] P. Glasenapp, D. S. Smirnov, A. Greilich, J. Hackmann, M. M. Glazov, F. B. Anders, and M. Bayer, Phys. Rev. B **93**, 205429 (2016).

[16] S. Varwig, A. Schwan, D. Barmscheid, C. Müller, A. Greilich, I. A. Yugova, D. R. Yakovlev, D. Reuter, A. D. Wieck, and M. Bayer, Phys. Rev. B **86**, 075321 (2012).

[17] A. Greilich, D. R. Yakovlev, and M. Bayer, in *Optical Generation and Control of Quantum Coherence in Semiconductor Nanostructures*, edited by G. Slavcheva and P. Roussignol (Springer, Berlin, 2010), Chap. 6.

[18] A. Greilich, M. Schwab, T. Berstermann, T. Auer, R. Oulton, D. R. Yakovlev, M. Bayer, V. Stavarache, D. Reuter, and A. Wieck, Phys. Rev. B **73**, 045323 (2006).

[19] For p-type QDs we also get $g_{zz}^{\mathrm{T}} = -0.4$, $\omega_N^{\mathrm{T}} = 70$ MHz, $\lambda^{\mathrm{T}} = 1$ (see the discussion in the main text). For n-type QDs we get $g_{zz}^{\mathrm{T}} = -0.45$, $\omega_N^{\mathrm{T}} = 16$ MHz, $\lambda^{\mathrm{T}} = 5$, $\tau_s^{\mathrm{T}} = 0.1$ μs. However, these parameters weakly affect the results. The longitudinal g-factors were also studied in Refs. [34,35].

[20] M. Y. Petrov, G. G. Kozlov, I. V. Ignatiev, R. V. Cherbunin, D. R. Yakovlev, and M. Bayer, Phys. Rev. B **80**, 125318 (2009).

[21] Y. Li, N. Sinitsyn, D. L. Smith, D. Reuter, A. D. Wieck, D. R. Yakovlev, M. Bayer, and S. A. Crooker, Phys. Rev. Lett. **108**, 186603 (2012).

[22] D. Heiss, S. Schaeck, H. Huebl, M. Bichler, G. Abstreiter, J. J. Finley, D. V. Bulaev, and D. Loss, Phys. Rev. B **76**, 241306 (2007).

[23] In the case of Ref. [22] the spin states are measured after a long dark period, while in other techniques the periodic excitation influences the system on shorter timescales.

[24] B. Urbaszek, X. Marie, T. Amand, O. Krebs, P. Voisin, P. Maletinsky, A. Högele, and A. Imamoglu, Rev. Mod. Phys. **85**, 79 (2013).

[25] I. A. Merkulov, A. L. Efros, and M. Rosen, Phys. Rev. B **65**, 205309 (2002).

[26] J. S. Colton, D. Meyer, K. Clark, D. Craft, J. Cutler, T. Park, and P. White, J. Appl. Phys. **112**, 084307 (2012).

[27] F. Fras, F. Bernardot, B. Eble, M. Bernard, B. Siarry, A. Miard, A. Lemaître, C. Testelin, and M. Chamarro, J. Phys.: Condens. Matter **25**, 202202 (2013).

[28] M. M. Glazov, Phys. Rev. B **91**, 195301 (2015).

[29] $\lambda = 1$ describes the fully isotropic case.

[30] P. Desfonds, B. Eble, F. Fras, C. Testelin, F. Bernardot, M. Chamarro, B. Urbaszek, T. Amand, X. Marie, J. M. Gérard *et al.*, Appl. Phys. Lett. **96**, 172108 (2010).

[31] J. Hackmann, P. Glasenapp, A. Greilich, M. Bayer, and F. B. Anders, Phys. Rev. Lett. **115**, 207401 (2015).

[32] V. S. Zapasskii, Adv. Opt. Photonics **5**, 131 (2013).

[33] J. Hübner, F. Berski, R. Dahbashi, and M. Oestreich, Phys. Status Solidi B **251**, 1824 (2014).

[34] I. A. Yugova, A. Greilich, E. A. Zhukov, D. R. Yakovlev, M. Bayer, D. Reuter, and A. D. Wieck, Phys. Rev. B **75**, 195325 (2007).

[35] A. Schwan, B.-M. Meiners, A. Greilich, D. R. Yakovlev, A. D. B. Maia, A. A. Quivy, A. B. Henriques, and M. Bayer, Appl. Phys. Lett. **99**, 221914 (2011).